DALTON
FULL PAPER

Polynuclear osmium–dioxolene complexes: comparison of electrochemical and spectroelectrochemical properties with those of their ruthenium analogues

Anita M. Barthram, Zöe R. Reeves, John C. Jeffery and Michael D. Ward *†

School of Chemistry, University of Bristol, Cantock's Close, Bristol, UK BS8 1TS. E-mail: mike.ward@bristol.ac.uk

Received 19th June 2000, Accepted 31st July 2000
Published on the Web 23rd August 2000

Reaction of $[Os(bipy)_2Cl_2]$ (bipy = 2,2′-bipyridine) with the poly-dioxolene ligands 3,4,3′,4′-tetrahydroxybiphenyl (H_4L^1), 2,3,6,7-trihydroxy-9-phenylxanthen-3-one (H_3L^2) or 2,3,6,7,10,11-hexahydroxytriphenylene (H_6L^3) afforded the complexes $[\{Os(bipy)_2\}_2(\mu\text{-}L^1)][PF_6]_2$, $[\{Os(bipy)_2\}_2(\mu\text{-}L^2)][PF_6]_3$, and the trinuclear complex $[\{Os(bipy)_2\}_3(\mu\text{-}L^3)][PF_6]_3$ abbreviated as $[\mathbf{Os_2}(L^1)]^{2+}$, $[\mathbf{Os_2}(L^2)]^{3+}$ and $[\mathbf{Os_2}(L^3)]^{3+}$, respectively. In these complexes two or three $\{Os^{III}(bipy)_2(OO)\}$ fragments are linked by the conjugated bridging ligands (where OO denotes a dioxolene binding site in any oxidation state). The complexes exhibit rich electrochemical behaviour, displaying a combination of metal-centred Os^{III}–Os^{II} couples (as reductions) and ligand-centred couples (as oxidations). UV/VIS/NIR spectroelectrochemical analysis was carried out on all three complexes in all accessible oxidation states, and the spectra were assigned with reference to the mononuclear model complex $[Os^{III}(bipy)_2(cat)][PF_6]$ (H_2cat = catechol) which was also examined spectroelectrochemically, as well as being crystallographically characterised. The comparison with the previously described ruthenium analogues is interesting due to their different internal oxidation state distribution. Whereas the mononuclear complex $[Os^{III}(bipy)_2(cat)]^+$ contains Os^{III} co-ordinated to a catecholate (oxidised metal, reduced ligand), the ruthenium analogue in the same oxidation state is $[Ru^{II}(bipy)_2(sq)]^+$ (sq = 1,2-benzosemiquinone monoanion), *i.e.* reduced metal and oxidised ligand. The same pattern of behaviour persists in the dinuclear and trinuclear complexes, and leads to interesting differences in the electrochemical properties of the ruthenium and osmium congeners.

Introduction

Complexes of the chelating dioxolene ligand series (catecholate(2−), semiquinonate(1−) and quinone; hereafter abbreviated as cat, sq and q, respectively) with numerous metals have been studied extensively.[1–3] A major focus of this interest is in the internal charge distribution of the complexes,[4–12] because extensive mixing of metal-based and ligand-based orbitals means that oxidation state assignments for metal and ligand are not always clear and can even undergo 'redox isomerism' as two forms interchange.[4,5]

Amongst these, the complexes of ruthenium and osmium have received particular attention because of their rich electrochemical and spectroscopic properties which allows the internal charge distribution to be studied in many different oxidation states.[6–12] For example, in the $[Ru(bipy)_2(OO)]^{n+}$ series [where 'OO' denotes a dioxolene ligand without specifying oxidation state; $n = 0$, 1 or 2] the ruthenium centre is in the +2 oxidation state throughout, with the different oxidation states arising from ligand-based redox processes between the catecholate, semiquinonate and quinone forms. The +1 form is therefore formulated as $[Ru^{II}(bipy)_2(sq)]^+$ on the basis of structural and spectroscopic evidence.[6,7] In contrast, in the osmium analogues $[Os(bipy)_2(OO)]^{n+}$ the greater ease of oxidation of osmium compared to ruthenium means that the +1 form is best described as $[Os^{III}(bipy)_2(cat)]^+$, on the basis of a crystal structure as well as EPR and UV/VIS/NIR spectroscopic data.[10]

We have recently been interested in linking several $[Ru(bipy)_2(OO)]^{n+}$ units together by use of bridging ligands containing two or more dioxolene binding sites. This has resulted in a series of polynuclear complexes displaying exceptionally rich electrochemical and spectroscopic behaviour.[13–17] The relevant ligands as shown above. Our interest in these is twofold. First, the large number of ligand-centred and/or metal-centred redox couples means that the complexes exist as extensive redox chains. Secondly, the electronic spectra of these complexes can, in some oxidation states, display very strong metal-to-ligand charge-transfer transitions in the near-infrared region of the spectrum which are of interest to us as dyes for electro-optic switching.[18–20] Both of these aspects are illustrated by the complex $[\{Ru(bipy)_2\}(L^1)]^{2+}$ which we described a few years ago.[13] The complex undergoes four reversible ligand-centred redox couples linking the components of a five-membered redox

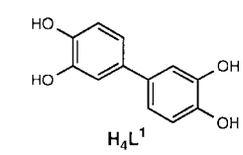

H_4L^1

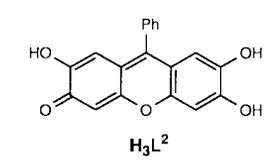

H_3L^2

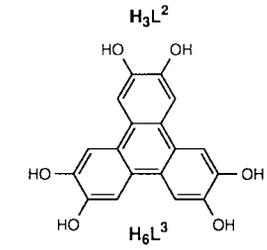

H_6L^3

† Royal Society of Chemistry Sir Edward Frankland fellow for 2000/2001.

 DOI: 10.1039/b004858p

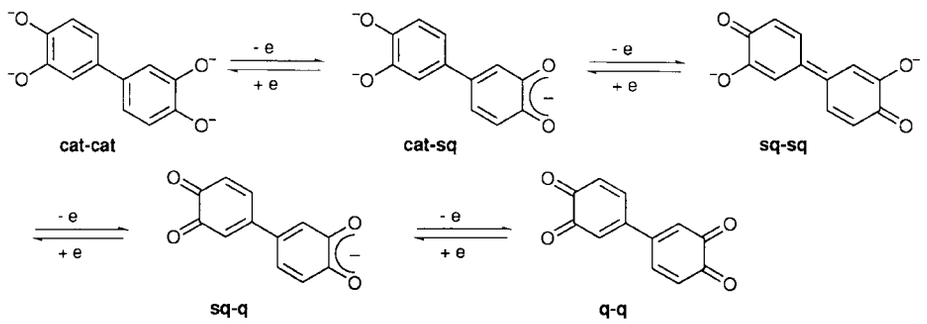

Scheme 1 The five-membered redox chain $[L^1]^{n+}$ ($n = -2$ to $+2$).

chain, in which the bridging ligand can exist in the oxidation states cat–cat, cat–sq, sq–sq, sq–q and q–q (Scheme 1). A spectroelectrochemical investigation revealed the presence of intense Ru^{II}→bridging ligand MLCT transitions in the near-IR region of the spectrum when the bridging ligand was in the sq–sq and sq–q oxidation states. An additional interesting feature of the complex is that the central biphenyl unit is twisted in the cat–cat and q–q oxidation states because of a formal single bond between the rings, but in the intermediate sq–sq state a diamagnetic quinonoidal structure arises with a double bond between the rings. The conformation of the conjugated pathway linking the two metals is therefore redox-switchable.

The results from our electrochemical and spectroscopic studies of these polynuclear ruthenium–dioxolene complexes have prompted us to extend our investigations to the osmium analogues. Although they will have the same basic structures and are formally isoelectronic with the ruthenium complexes, the different internal charge distribution in the oxidised states [*i.e.* Os^{III}(cat) *vs.* Ru^{II}(sq)] results in significantly different electrochemical and spectroscopic properties. In particular, comparison of the electrochemical properties of the related complexes of Ru and Os proved to be particularly useful in helping to assign individual redox processes as metal- or ligand-centred.

We describe here the syntheses, electrochemical and spectroelectrochemical properties of the dinuclear complexes $[\{Os(bipy)_2\}_2(\mu\text{-}L^1)][PF_6]_2$, $[\{Os(bipy)_2\}_2(\mu\text{-}L^2)][PF_6]_3$, and the trinuclear complex $[\{Os(bipy)_2\}_3(\mu\text{-}L^3)][PF_6]_3$ together with comparative studies on the mononuclear model complex $[Os(bipy)_2(cat)][PF_6]$.[10] These polynuclear complexes are abbreviated as $[\mathbf{Os_2}(L^1)]^{2+}$, $[\mathbf{Os_2}(L^2)]^{3+}$ and $[\mathbf{Os_3}(L^3)]^{3+}$ respectively, where **Os** denotes the $\{Os(bipy)_2\}$ fragment.

Results and discussion

The mononuclear model complex $[Os(bipy)_2(cat)][PF_6]$

This complex was described a while ago by Haga, Pierpont and co-workers;[10] we have prepared and re-investigated it so that reference electrochemical and spectroscopic data were recorded on the same instruments and under the same conditions as used for the new polynuclear complexes. It was not structurally characterised when originally prepared, although its substituted analogue $[Os(bipy)_2(3,5\text{-}^tBu_2cat)][ClO_4]$ was.[10]

Crystals of $[Os(bipy)_2(cat)][PF_6]$ were obtained by slow evaporation from MeCN, and the crystal structure of the complex is shown in Fig. 1. The complex cation lies on a C_2 axis which passes through the centre of the catecholate ligand and through the Os atom. The structure is basically as expected for a pseudo-octahedral tris-chelate but a couple of points are worthy of comment. The Os–O and O–C bond distances are the most significant features of this structure, as they are strongly diagnostic of the charge distribution in the complex.[10] In the Os^{III}(cat) description the C–O bonds are formally single and therefore longer than in semiquinone complexes.[21] Similarly, the strong electrostatic interaction between Os^{3+} and O^-, and the

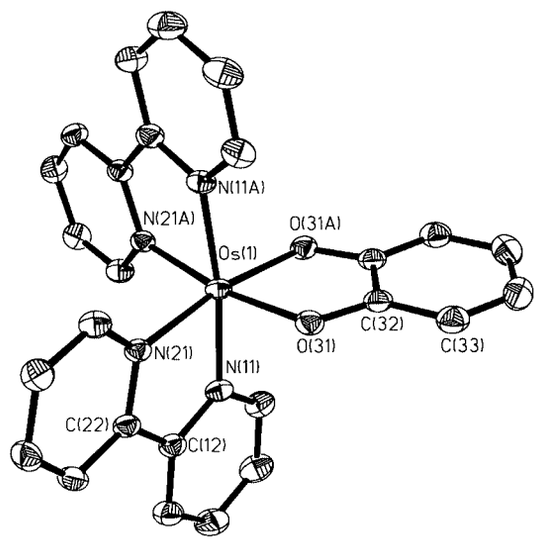

Fig. 1 Crystal structure of the complex cation of $[Os(bipy)_2(cat)][PF_6]$ (thermal ellipsoids at 40% probability level). Selected bond distances (Å) and angles (°): Os(1)–O(31) 2.018(2), Os(1)–N(21) 2.058(3), Os(1)–N(11) 2.061(3), O(31)–C(32) 1.345(4); O(31)–Os(1)–O(31A) 81.46(13), O(31)–Os(1)–N(21A) 170.55(9), O(31)–Os(1)–N(21) 91.50(10), N(21)–Os(1)–N(21A) 96.16(15), N(11)–Os(1)–O(31) 90.65(10), N(11)–Os(1)–N(21) 78.38(11), O(31)–Os(1)–N(11A) 95.32(10) and N(21)–Os(1)–N(11A) 96.30(10).

smaller size of the more highly oxidised metal centre, result in a shorter Os–O bond than would be expected for the Os^{II}(sq) valence isomer.[11] The lengths of the C–O bonds in the dioxolene ligand [C(32)–O(31), 1.345(4) Å] and of the Os–O bonds [Os(1)–O(31), 2.018(2) Å] are both entirely consistent with the Os^{III}(cat) formulation that was also apparent for $[Os(bipy)_2(3,5\text{-}^tBu_2cat)][ClO_4]$.[10]

Cyclic and square-wave voltammetry of $[Os(bipy)_2(cat)][PF_6]$ in MeCN gave results which were very similar to those reported earlier (measured in 1,2-dichloroethane),[10] with a reversible one-electron reduction at −0.78 V and reversible one-electron oxidation at 0.00 V, both *vs.* Fc–Fc^+ (Table 1).[10] This may be compared with redox potentials of −0.69 and +0.16 V *vs.* Fc–Fc^+ for the ruthenium analogue measured in our lab under the same conditions, which are assigned[6] to dioxolene-centred cat–sq and sq–q processes respectively giving Ru^{II}(sq) and Ru^{II}(q) species. Despite the similarity of the redox potential values between the ruthenium and osmium complexes, the assignments are different as mentioned above, with the first oxidation of the osmium complex being metal-centred to give an Os^{III}(cat) complex. The second redox process has tentatively been assigned as ligand based, giving Os^{III}(sq),[10] although in principle a second metal-based oxidation to give Os^{IV}(cat) is also possible. This ambiguity has been resolved by the study of the polynuclear complexes described below which shows that in them at least the second oxidation at each site is indeed ligand-centred.

Table 1 Electrochemical data for the new osmium complexes and their ruthenium analogues

Complex	E^a/V						
$[Os(bipy)_2(cat)][PF_6]$	−0.78	+0.00	+1.07 [b]				
$[Ru(bipy)_2(sq)][PF_6]$ [c]	−0.69	+0.16	+1.24 [b]				
$[\mathbf{Os_2}(L^1)]^{2+}$	−0.78 [d]	−0.68 [d]	−0.11	+0.23			
$[\mathbf{Ru_2}(L^1)]^{2+}$ [c]	−1.04	−0.70	+0.06	+0.38			
$[\mathbf{Os_2}(L^2)]^{3+}$	−0.48	−0.33	+0.43	+0.88 [b]			
$[\mathbf{Ru_2}(L^2)]^{+}$ [e]	−0.36	+0.00	+0.53	+1.30 [b]			
$[\mathbf{Os_3}(L^3)]^{3+}$	[f]	[f]	[f]	−0.18	+0.12	+0.42	+1.04 [b]
$[\mathbf{Ru_3}(L^3)]^{3+}$ [g]	−0.97	−0.70	−0.43	−0.03	+0.36	+0.66	

[a] Potentials are quoted *vs.* internal ferrocene–ferrocenium. Measurements were made in MeCN at platinum electrode with a scan rate of 0.2 V s^{-1}. All processes are reversible except where indicated otherwise. [b] Irreversible process. [c] Ref. 13. [d] Apparently symmetric waves in a cyclic voltammogram, but irreversible on the slow timescale of spectroelectrochemistry. [e] Ref. 16. [f] Apparently irreversible processes obscured by intense stripping peaks. [g] Ref. 15.

Table 2 Electronic spectra of the new osmium complexes in all accessible oxidation states (MeCN, −30 °C) (sh = shoulder)

Complex	λ_{max}/nm [10^{-3} ε/dm^3 mol^{-1} cm^{-1}]								
$[Os^{II}(bipy)_2(cat)]$			920 (sh)	807 (6.0)	596 (8.5)	498 (10)	411 (10)	291 (41)	243 (34)
$[Os^{III}(bipy)_2(cat)]^+$	2000 (0.5)	1513 (0.7)	807 (10)		494 (7.2)		358 (9.1)	290 (47)	244 (32)
$[Os^{III}(bipy)_2(sq)]^{2+}$			800 (1.0)	638 (sh)	539 (11)	462 (7.5)	410 (6.0)	289 (37)	249 (34)
$[\mathbf{Os_2}(L^1)]^{2+}$	1930 (2.5)	1480 (2.1)	961 (14)			494 (8.6)		291 (59)	242 (44)
$[\mathbf{Os_2}(L^1)]^{3+}$	1910 (4.0)	1600 (7.5)	1186 (14)	900 (sh)	689 (8.2)		391 (14)	289 (55)	243 (43)
$[\mathbf{Os_2}(L^1)]^{4+}$	1920 (1.7)	1400 (1.6)	892 (9.0)	733 (17)	598 (sh)	490 (7.6)		289 (49)	247 (44)
$[\mathbf{Os_2}(L^2)]^{1+}$				727 (26)	589 (20)	463 (15)	419 (16)	295 (62)	244 (48)
$[\mathbf{Os_2}(L^2)]^{2+}$		1740 (2.4)	850 (sh)	725 (17)	576 (17)	463 (14)		292 (59)	244 (28)
$[\mathbf{Os_2}(L^2)]^{3+}$		1685 (0.9)	895 (7.0)	730 (19)	609 (21)	555 (19)	439 (13)	289 (59)	244 (49)
$[\mathbf{Os_2}(L^2)]^{4+}$	1920 (4.4)	1750 (5.2)	1250 (3.4)	910 (sh)	806 (8.0)	639 (23)	412 (11)	288 (51)	246 (46)
$[\mathbf{Os_3}(L^3)]^{3+}$	1660 (2.8)			1069 (35)	657 (sh)	488 (sh)	340 (39)	292 (120)	244 (84)
$[\mathbf{Os_3}(L^3)]^{4+}$				1000 (42)		462 (18)	350 (36)	291 (120)	244 (85)
$[\mathbf{Os_3}(L^3)]^{5+}$		1370 (12)	1050 (13)	741 (36)			350 (33)	289 (110)	245 (87)
$[\mathbf{Os_3}(L^3)]^{6+}$	1150 (sh)	1000 (sh)	820 (sh)	705 (36)			364 (27)	287 (99)	249 (91)

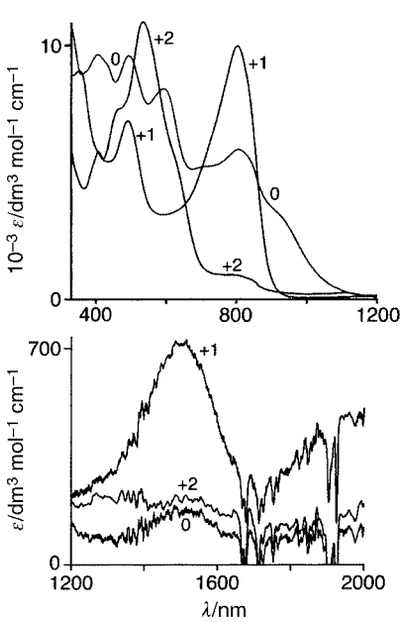

Fig. 2 Electronic spectra of $[Os(bipy)_2(cat)]^{n+}$ ($n = 0$, 1 or 2) measured during a spectroelectrochemical experiment in MeCN at −30 °C.

The results of a spectroelectrochemical study on the redox series $[Os(bipy)_2(cat)]^{n+}$ ($n = 0$, 1 or 2) in MeCN at −30 °C are shown in Fig. 2 (see also Table 2) and are in good agreement with the data published for $[Os(bipy)_2(3,5\text{-}^tBu_2cat)][ClO_4]$ measured in CH_2Cl_2.[10] Tentative assignments for some of these are included in Table 2. On oxidation of the fully reduced complex ($n = 0$) to the monocation ($n = 1$) the MLCT transitions at 411, 498 and 596 nm disappear and are replaced by π(bipy) →Os^{III} and π(cat)→Os^{III} transitions at 494 and 807 nm respectively. In addition weak transitions appear at 1513 nm and *ca.* 2000 nm, whose position and intensity are consistent with metal-centred d–d transitions within the d(π) manifold, arising from the low symmetry of the complex which splits the members of the 't_{2g}' orbital set.[22] This provides excellent confirmatory evidence for the description of the mono-oxidised complex as Os^{III}(cat) (*cf.* the crystal structure). Further oxidation (to $n = 2$) results in collapse of the π(cat)→Os^{III} LMCT transition and its replacement by a higher-energy transition at 539 nm, assigned as a π(sq)→Os^{III} LMCT following ligand-centred oxidation.[10] Since oxidation of cat to sq will result in its orbitals being lowered in energy, we would expect the resultant LMCT transition to be blue-shifted and this is indeed the case.

Polynuclear complexes: synthesis and characterisation

The three polynuclear osmium complexes were prepared in the same way as their ruthenium congeners, by reaction of the bridging ligand with the appropriate number of equivalents of $[Os(bipy)_2Cl_2]$ in the presence of base. The greater kinetic inertness of Os^{II} compared to Ru^{II} meant that reactions were slow and yields sometimes poor, with numerous side-products being detected by thin-layer chromatography. Following chromatographic purification the complexes were characterised on the basis of their electrospray mass spectra and elemental analyses. Electrospray mass spectra were especially useful, confirming not only the molecular weight of the complex cation but also the charge. This is necessary in complexes where the presence of multiple redox processes at modest potentials (see later) means that it is not always obvious in which oxidation state a complex is isolated. For example, the complex with H_3L^2 was found to be $[\mathbf{Os_2}(L^2)][PF_6]_3$ because the electrospray mass spectrum showed a strong peak at *m*/*z* 439.7 corresponding to $(M - 3PF_6)^{3+}$. Elemental analyses of the polynuclear complexes consistently gave rather low %C and %N values, a problem which is in our experience common for polynuclear complexes of heavy metals with extended, highly aromatic ligands. This can partially be

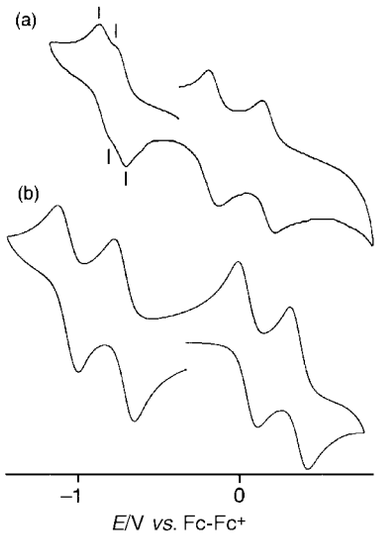

Fig. 3 Cyclic voltammograms of (a) $[\mathbf{Os_2}(L^1)]^{2+}$ and (b) $[\mathbf{Ru_2}(L^1)]^{2+}$ in MeCN (platinum working electrode; scan rate 0.2 V sec^{-1}).

accounted for by assuming the presence of water of crystallisation; however it is also likely that the complexes are particularly refractory and do not undergo complete combustion despite the addition of burning aids such as V_2O_5.

We were unable to obtain either NMR or EPR data for these complexes. The absence of NMR spectra is to be expected for osmium(III) complexes; the absence of EPR spectra at 77 K may be explained by the presence of two or three paramagnetic centres which would result in fast relaxation leading to broad, weak signals.

Electrochemical properties of the osmium complexes and comparison with their ruthenium analogues

$[\mathbf{Os_2}(L^1)]^{2+}$. Cyclic and square-wave voltammetry on $[\mathbf{Os_2}(L^1)]^{2+}$ in MeCN revealed the presence of four reversible one-electron redox processes at +0.23, −0.11, −0.68 and −0.78 V *vs.* Fc–Fc^+, *i.e.* $[\mathbf{Os_2}(L^1)]^{2+}$ is the central member of a five-membered redox series in which the charge on the complex varies from 0 to +4 [Fig. 3(a)]. With respect to the +2 state in which the complex is isolated, the first two processes are oxidations and the latter two are reductions. The one-electron nature of the two well separated oxidations ($\Delta E_{1/2}$ = 340 mV) is established by the peak–peak separations of 60–70 mV. The two reductions overlap closely in the cyclic voltammogram ($\Delta E_{1/2}$ = 100 mV), so the half-wave potentials were taken from the peaks of the square-wave voltammogram. The one-electron nature of these two processes follows from the fact that all four peaks in the square-wave voltammogram are of about the same intensity.

Sharp stripping peaks associated with the return waves of these reduction processes were apparent during some experiments, suggesting adsorption of the reduced species on to the platinum electrode surface, but their intensity and position seemed to vary randomly and they were not present at all on occasion [*cf.* Fig. 3(a)]. In fact the reductions proved to be irreversible during spectroelectrochemical measurements (see later), presumably because of this adsorption problem.

Assigning these processes as metal- or ligand-centred is greatly facilitated by comparison with the analogous ruthenium complex $[\mathbf{Ru_2}(L^1)]^{2+}$ [Fig. 3(b)].[13] For this complex the four redox processes occur at +0.38, +0.06, −0.70 and −1.04 V *vs.* Fc–Fc^+, and are all assignable as ligand-centred (Scheme 1). The separation between the two sq–q couples is 320 mV, and between the two cat–sq couples is 340 mV. These substantial redox separations reflect the fact that the redox sites are close together and therefore strongly interacting,[23] and the excellent agreement between the two $\Delta E_{1/2}$ values is good evidence that

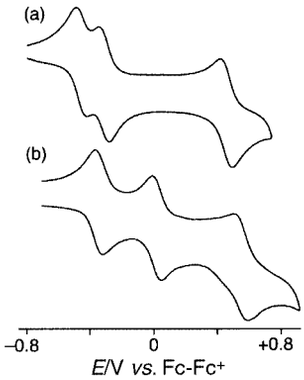

Fig. 4 Cyclic voltammograms of (a) $[\mathbf{Os_2}(L^2)]^{3+}$ and (b) $[\mathbf{Ru_2}(L^2)]^{+}$ in MeCN (platinum working electrode; scan rate 0.2 V s^{-1}). The irreversible oxidation at high positive potential is not shown.

the pair of oxidations and the pair of reductions are both ligand centred and therefore interacting to about the same extent. For $[\mathbf{Os_2}(L^1)]^{2+}$ the 340 mV separation between the two oxidations is in very close agreement with the $\Delta E_{1/2}$ values observed for $[\mathbf{Ru_2}(L^1)]^{2+}$, providing strong confirmation that these processes are also ligand-centred in the osmium complex. However the greatly reduced redox splitting of $\Delta E_{1/2}$ = 100 mV between the reductions of $[\mathbf{Os_2}(L^1)]^{2+}$ indicates that the two redox processes are spatially further apart, and must therefore be in more predominantly metal-centred orbitals. This observation provides convincing support for the proposed behaviour of mononuclear $[Os^{II}(bipy)_2(cat)]$ in which it was suggested that the first oxidation is metal based to give $[Os^{III}(bipy)_2(cat)]^+$, and the second is ligand-based to give $[Os^{III}(bipy)_2(sq)]^{+}$.[10] The best formulation for $[\mathbf{Os_2}(L^1)]^{2+}$ is therefore $[(bipy)_2Os^{III}(cat–cat)Os^{III}(bipy)_2]^{2+}$, in contrast to $[\mathbf{Ru_2}(L^1)]^{2+}$ which is formulated as $[(bipy)_2Ru^{II}(sq–sq)Ru^{II}(bipy)_2]^{2+}$.[13]

$[\mathbf{Os_2}(L^2)]^{3+}$. Comparison of the electrochemical behaviour of $[\mathbf{Os_2}(L^2)]^{3+}$ with that of the ruthenium analogue $[\mathbf{Ru_2}(L^2)]^{+}$ was likewise helpful in assigning the redox processes.[16] Note that this osmium complex was isolated with an overall charge of +3, in contrast to $[\mathbf{Ru_2}(L^2)]^{+}$ which was isolated in its fully reduced +1 state; of course this does not affect its electrochemical behaviour as the interconversions are reversible. Complex $[\mathbf{Os_2}(L^2)]^{3+}$ shows reversible one-electron redox couples at +0.43, −0.33 and −0.48 V [Fig. 4(a)], as well as an irreversible oxidation at +0.88 V *vs.* Fc–Fc^+ . For $[\mathbf{Ru_2}(L^2)]^{+}$ the three reversible processes occur at +0.53, 0.00 and −0.36 V [Fig. 4(b)], with the irreversible oxidation at +1.30 V. Considering the three reversible processes, we can immediately see that the two more negative processes (which are reductions for $[\mathbf{Os_2}(L^2)]^{3+}$) are closer together for $[\mathbf{Os_2}(L^2)]^{3+}$ ($\Delta E_{1/2}$ = 150 mV) than for $[\mathbf{Ru_2}(L^2)]^{+}$ ($\Delta E_{1/2}$ = 360 mV). For $[\mathbf{Ru_2}(L^2)]^{+}$ we used ZINDO calculations to show that the frontier orbitals concerned were strongly delocalised over metals and bridging ligand, with a substantial ligand-centred component. For $[\mathbf{Os_2}(L^2)]^{3+}$, as with $[\mathbf{Os_2}(L^1)]^{2+}$ above, the reduced separation between the potentials of these two couples compared to that of the ruthenium analogue confirms that they are in more metal-centred orbitals, with the greater spatial separation between the redox centres resulting in a reduced $\Delta E_{1/2}$ value. We therefore ascribe the final reversible couple at +0.43 V (an oxidation compared to the starting state) to a bridging-ligand-centred process. The nature of the high-potential irreversible process is not clear: it could be an Os^{III}–Os^{IV} couple or a second ligand-centred couple.

$[\mathbf{Os_3}(L^3)]^{3+}$. The redox properties of $[\mathbf{Os_3}(L^3)]^{3+}$ are compared with those of $[\mathbf{Ru_3}(L^3)]^{3+}$ in Fig. 5. In $[\mathbf{Ru_3}(L^3)]^{3+}$ each ligand binding site is formally in a mononanionic semiquinone oxidation state, such that the complex is denoted $Ru^{II}{}_3$(sq,sq,sq)

(Fig. 6).[15] As with $[\mathbf{Ru_2}(L^1)]^{2+}$, which is diamagnetic because of spin pairing between the two semiquinone sites (Scheme 1), $[\mathbf{Ru_3}(L^3)]^{3+}$ is only a monoradical because any two of the three semiquinone sites can pair up to give an additional double bond (Fig. 6). Electrochemical studies on $[\mathbf{Ru_3}(L^3)]^{3+}$ revealed six (ligand-centred) redox processes linking seven oxidation states, from Ru^{II}_3(cat,cat,cat) to Ru^{II}_3(q,q,q); of these only the three most positive, from Ru^{II}_3(sq,sq,sq) up to Ru^{II}_3(q,q,q), were fully reversible, with potentials of +0.66, +0.36 and −0.03 V *vs.* Fc–Fc^+. As in the dinuclear complexes, the substantial separation between successive redox processes (300 and 330 mV, respectively) can be taken as evidence of their ligand-centred nature.

For $[\mathbf{Os_3}(L^3)]^{3+}$, based on the arguments used for the two dinuclear complexes about internal assignment of oxidation states, the formulation Os^{III}_3(cat,cat,cat) is likely for the 3+ state in which the complex is isolated [in contrast to Ru^{II}_3(sq,sq,sq) for the ruthenium analogue]. We might therefore expect to see three metal-centred Os^{III}–Os^{II} reductions and three ligand-centred cat–sq oxidations, with the metal-centred processes being close together and the ligand-centred processes being more highly separated (*cf.* the behaviour of $[\mathbf{Os_2}(L^1)]^{2+}$). Unfortunately the processes at negative potentials were irreversible and obscured by strong stripping peaks to the extent that it is not possible even to count the number of processes. However, the three expected oxidations are apparent (Fig. 5) at +0.42, +0.12 and −0.18 V *vs.* Fc–Fc^+, and the successive redox separations of 300 mV are in excellent agreement with the behaviour of $[\mathbf{Ru_3}(L^3)]^{3+}$, confirming the ligand-centred nature of these processes. Whereas for $[\mathbf{Ru_3}(L^3)]^{3+}$ the three oxidations are sq–q couples resulting in Ru^{II}_3(q,q,q) with a charge of +6, for $[\mathbf{Os_3}(L^3)]^{3+}$ they must be cat–sq couples resulting ultimately in the Os^{III}_3(sq,sq,sq) species with a charge of +6 (Fig. 6).

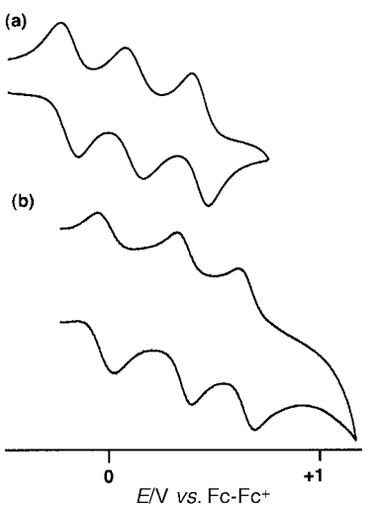

Fig. 5 Cyclic voltammograms of (a) $[\mathbf{Os_3}(L^3)]^{3+}$ and (b) $[\mathbf{Ru_3}(L^3)]^{3+}$ in MeCN (platinum working electrode; scan rate 0.2 V s^{-1}).

Spectroelectrochemical properties of the complexes

$[\mathbf{Os_2}(L^1)]^{n+}$ (n = 2, 3 or 4). A spectroelectrochemical study in MeCN at 243 K (Fig. 7) allowed measurement of the electronic spectrum of this complex in the three higher oxidation states $[\mathbf{Os_2}(L^1)]^{n+}$ (n = 2, 3 or 4). Attempts to perform the reductions in the OTTLE cell resulted in slow precipitation of the reduced material so unfortunately it was not possible to record the spectra of the reduced states.

The spectrum of $[\mathbf{Os_2}(L^1)]^{2+}$ may be assigned by comparison with mononuclear $[Os(bipy)_2(cat)]^+$ (see above); the principal lowest-energy transition at 961 nm (ε = 14,000 dm^3 mol^{-1} cm^{-1}) is a π(cat)→Os^{III} LMCT, analogous to the transition at 807 nm for $[Os(bipy)_2(cat)]^+$. In addition the two low-energy transitions

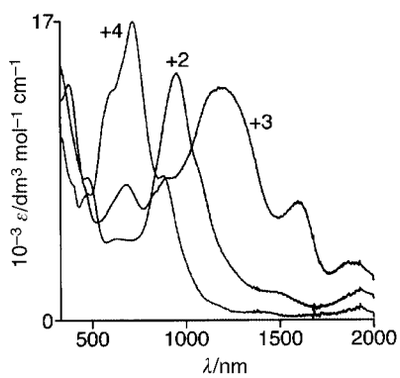

Fig. 7 Electronic spectra of $[\mathbf{Os_2}(L^1)]^{n+}$ (n = 2, 3 or 4) measured during a spectroelectrochemical experiment in MeCN at −30 °C. Spectra of the n = 0 and 1 states could not be recorded due to deposition of the reduced forms of the complex on the electrode surface.

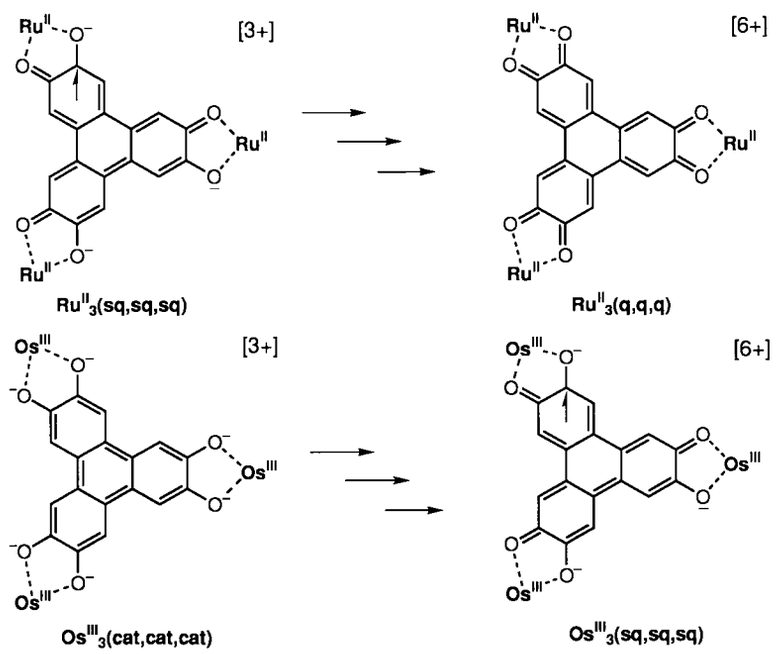

Fig. 6 Comparison of ligand-centred (sq ⟶ q) oxidations of $[\mathbf{Ru_3}(L^3)]^{3+}$ with metal-centred [Os^{II} ⟶ Os^{III}] oxidations of $[\mathbf{Os_3}(L^3)]^{3+}$.

of $[\mathbf{Os_2}(L^1)]^{2+}$ at 1480 and 1930 nm are comparable to the d–d transitions of $[Os(bipy)_2(cat)]^+$ (1513 and 1992 nm), although they are rather more intense with absorption coefficients of >2000 $dm^3\ mol^{-1}\ cm^{-1}$; this could be due either to intensity borrowing from the LMCT process at 961 nm, or to a greater degree of Os/dioxolene orbital mixing resulting in partial charge-transfer character for the 'd–d' transitions. In the fully oxidised form $[\mathbf{Os_2}(L^1)]^{4+}$ the π(cat)→Os^{III} LMCT has been replaced by a π(sq)→Os^{III} LMCT at higher energy (733 nm; $\varepsilon = 17{,}000\ dm^3\ mol^{-1}\ cm^{-1}$), exactly in agreement with the behaviour of mononuclear $[Os^{II}(bipy)_2(cat)]^+$ whose π(cat)→Os^{III} LMCT at 807 nm is replaced by a π(sq)→Os^{III} transition at 539 nm on oxidation to $[Os^{III}(bipy)_2(sq)]^{2+}$.

The behaviour of the mixed-valence state $[\mathbf{Os_2}(L^1)]^{3+}$ is less obvious. On the basis that the oxidation is ligand-centred, the mixed-valence state may be described as {Os^{III}(sq–cat)Os^{III}} with the ligand termini in different oxidation states. The question then arises as to whether the ligand is delocalised and planar such that each terminus is equivalent, or whether it is twisted about the central C–C bond with the two termini valence-localised. In the latter case we might expect distinct, identifiable π(cat)→Os^{III} and π(sq)→Os^{III} LMCT transitions from the inequivalent termini. In fact, this is not what happens: the principal low-energy transition moves to 1186 nm ($\varepsilon = 14{,}000\ dm^3\ mol^{-1}\ cm^{-1}$) and there are additional weaker transitions at 1600 and 1910 nm. This behaviour is more consistent with that expected from a planar, delocalised complex in which there is a single LMCT transition arising from the bridging ligands (50% cat and 50% sq character) to the Os^{III}, although why it should be at such low energy is not clear. We note that this is similar to the behaviour shown by the mixed-valence Ru^{II}(sq,q)Ru^{II} state in $[\mathbf{Ru_2}(L^1)]^{3+}$: a single MLCT transition was observed at lower energy than either of the individual Ru^{II}→sq or Ru^{II}→q transitions that would have been expected for a valence-localised system. The lower-energy transitions are therefore tentatively ascribable to intra-ligand processes involving the SOMO of the bridging ligand.[16,24]

$[\mathbf{Os_2}(L^2)]^{n+}$ (n = 1, 2, 3 or 4). The results of a spectroelectrochemical study of $[\mathbf{Os_2}(L^2)]^{n+}$ (n = 1 to 4) in MeCN at 243 K are shown in Fig. 8 (see also Table 2). We start with the complex in the +3 state in which it was isolated, with the metals both formally Os^{III} and the ligand present as the fully reduced $[L^2]^{3-}$. Assignment of the spectrum is assisted by comparison with mononuclear $[Os^{III}(bipy)_2(cat)]^+$. Thus, the weak transition in the near-IR region at 1685 nm is ascribable to a d–d transition of Os^{III}; this helps to confirm what was suggested by the electrochemistry, *viz.* that the two closely spaced redox couples at −0.48 and −0.33 V *vs.* $Fc–Fc^+$ are metal-centred. Between 430 and 900 nm is a collection of at least five transitions. By analogy with $[Os^{III}(bipy)_2(cat)]^+$ we expect both π(bipy)→Os^{III} and π($[L^2]^{3-}$)→Os^{III} LMCT transitions. The latter are expected to be at lower energy than the former but individual assignment of these transitions is not immediately obvious beyond the fact that they have LMCT character.

On one-electron reduction to the 2+ state, formally a mixed-valence Os^{II}/Os^{III} complex, the pattern of maxima in the visible (400–800 nm) region changes as the π(bipy)→Os^{III} LMCT transitions of one terminus are replaced by Os^{II}→bipy(π*) MLCT transitions in the same region.[25] In addition the absorbance in the near-IR region increases such that there is an almost constant absorbance with ε *ca.* 2000 $dm^3\ mol^{-1}\ cm^{-1}$ between 1200 and 2000 nm [the low-energy limit of the measurement; see Fig. 8(d)]. A maximum is just discernible at *ca.* 1740 nm which could be a d–d transition from the remaining osmium(III) centre. On further reduction to the 1+ state [Os^{II}/Os^{II}] this broad near-IR absorbance disappears; since it is present only in the mixed-valence Os^{II}/Os^{III} state it can confidently be assigned to one (or more, not well resolved) inter-valence charge-transfer transitions from Os^{II} to Os^{III}. For weakly coupled Os^{II}/Os^{III} complexes up to three inter-valence charge-transfer (IVCT) transitions are expected arising from the presence of three different acceptor levels in the osmium(III) terminus arising from the strong spin–orbit coupling, and semi-quantitative analyses of the positions of such transitions have been used to estimate the magnitude of spin–orbit coupling for several complexes.[26–28] In this case however the IVCT transitions are not sufficiently well resolved to allow such an analysis. In addition, there are further changes in the visible region of the spectrum consistent with replacement of the remaining π(bipy)→Os^{III} LMCT transitions with Os^{II}→bipy(π*) MLCT transitions.[25]

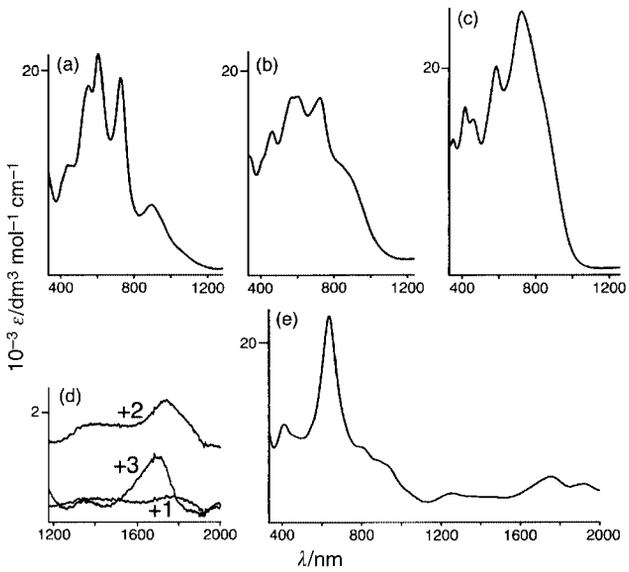

Fig. 8 Electronic spectra of $[\mathbf{Os_2}(L^2)]^{n+}$ (n = 1, 2, 3 or 4) measured during a spectroelectrochemical experiment in MeCN at −30 °C. For clarity the spectra are shown individually. (a) n = 3; (b) n = 2; (c) n = 1; (d) near-IR region of n = 3, 2, 1 states overlaid; (e) n = 4.

Oxidation of $[\mathbf{Os_2}(L^2)]^{3+}$ to $[\mathbf{Os_2}(L^2)]^{4+}$, which is assumed to involve oxidation of the bridging ligand,[16,24] results in two significant changes to the spectrum. First, the region between 400 and 1000 nm undergoes several changes, *viz.* the transition at 439 nm is blue-shifted to 412 nm; the three transitions at 555, 609 and 730 nm are replaced by a single more intense transition at 639 nm; and the transition at 895 nm is replaced by two at 806 and *ca.* 910 nm. These changes will principally be related to the collapse of π($[L^2]^{3-}$)→Os^{III} LMCT transitions and their replacement by π($[L^2]^{2-}$)→Os^{III} LMCT transitions; in contrast we expect the π(bipy)→Os^{III} LMCT transitions in this region to be relatively little affected. Secondly, a broad region of absorbance in the near-IR region, with a maximum at 1750 nm, can be ascribed to a new ligand-centred π ⟶ π* transition associated with the SOMO of the bridging ligand, *cf.* the behaviour of $[\mathbf{Ru_2}(L^1)]^{3+}$ (above), superimposed on the existing metal-centred d–d transitions. Similar behaviour was observed for both ruthenium[16] and nickel[24] complexes of L^2 in oxidation states where the bridging ligand had an odd electron count.

$[\mathbf{Os_3}(L^3)]^{n+}$ (n = 3, 4, 5 or 6). The results of a spectroelectrochemical study of $[\mathbf{Os_3}(L^3)]^{n+}$ (n = 3 to 6) in MeCN at 243 K are in Fig. 9 (see also Table 2). Starting with the complex in the +3 state as isolated, the internal oxidation state distribution is $Os^{III}{}_3$-(cat,cat,cat) and the intense near-IR absorption maximum at 1069 nm [$\varepsilon = 35{,}000\ dm^3\ mol^{-1}\ cm^{-1}$] may be ascribed to a cat→Os^{III} LMCT originating from the bridging ligand. For comparison, this occurs at 807 nm for mononuclear $[Os(bipy)_2$-$(cat)]^+$ and 961 nm for dinuclear $[\mathbf{Os_2}(L^1)]^{2+}$; as the charge on the dioxolene ligand increases from –2 (mononuclear complex) through –4 (dinuclear complex) to –6 (trinuclear complex), its HOMO becomes higher in energy and therefore the LMCT transition arising from the dioxolene HOMO is steadily red-

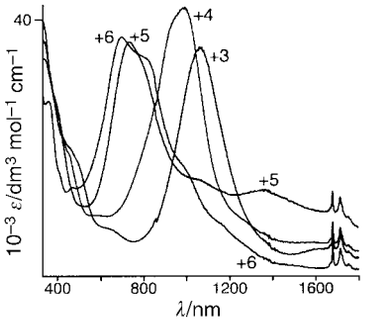

Fig. 9 Electronic spectra of $[\mathbf{Os_3}(L^3)]^{n+}$ ($n = 3$, 4, 5 or 6) measured during a spectroelectrochemical experiment in MeCN at −30 °C.

shifted. This transition tails off slowly through the near-IR region, but a just-discernible maximum at 1660 nm is characteristic of the osmium(III) centres as described earlier. The expected π(bipy)→Os^{III} LMCT transitions in the visible region, and bipy-centred π ⟶ π* transitions in the UV region, are also apparent.

The oxidation to give the +4 state is centred on the bridging ligand whose oxidation state may be described as [cat,cat,sq]. As with the dinuclear mixed-valence complex $[\mathbf{Os_2}(L^1)]^{2+}$ the question arises as to whether this is localised, giving distinct cat and sq ligand fragments, or delocalised to give three equivalent binding sites which are of mixed character. In this case the rigid planarity of the bridging ligand suggests that the latter is more likely, and indeed it is simple to use 'curly arrows' to show how the odd electron from the sq fragment can be delocalised equally to all three sites. In the electronic spectrum the result is that the LMCT transition originating from the bridging ligand is blue-shifted to 1000 nm, consistent with it having some sq→Os^{III} character (one third) in addition to cat→Os^{III} character (two thirds). Further oxidation to the +5 state, with the bridging ligand at the [cat,sq,sq] level, results in a further blue-shift of the low energy LMCT transition for the same reasons: it now has two thirds sq→Os^{III} character and only one third of cat→Os^{III} character. In addition there are lower-energy shoulders at 1370 and *ca.* 1050 nm whose nature is not obvious. Possibly they could arise as a result of the strong spin–orbit coupling which will result in any transitions involving the osmium(III) centre being split into several components, *cf.* the IVCT processes mentioned earlier for $[\mathbf{Os_2}(L^2)]^{2+}$.[26–28] Finally, oxidation to the +6 state to give the [sq,sq,sq] bridging ligand results in a further blue-shift of the LMCT absorption maximum to 705 nm (with pronounced lower-energy shoulders at 820, 1000 and *ca.* 1150 nm).

The steady decrease of the LMCT transition as the oxidations proceed is clear proof that the +4 and +5 mixed-valence states are fully delocalised. Exactly similar behaviour was shown by $\mathbf{Ru_3}(L^3)^{3+}$, whose oxidation state description is $Ru^{II}{}_3$-(sq,sq,sq) (Fig. 6).[15] In this case the three oxidations are sq–q couples, and as the oxidations proceed the Ru^{II}→sq MLCT transition to the (delocalised) bridging ligand steadily blue-shifts as it gains more and more Ru^{II}→q MLCT character. Although in the osmium complex the transitions are LMCT rather than MLCT in nature, the principle is identical.

Conclusion

Two dinuclear complexes and one trinuclear complex, containing $\{Os^{III}(bipy)_2(cat)\}^+$ fragments linked by a conjugated polydioxolene bridging ligand, have been prepared. Electrochemical studies clearly indicate that reductions are metal-centred Os^{III}–Os^{II} couples, whereas oxidations are ligand-centred sq–q couples. This is in interesting contrast to the ruthenium analogues for which the metal is much harder to oxidise and consequently ligand-centred processes dominate the redox chains. The assignments are supported by UV/VIS/NIR spectroelectrochemical studies, which show (amongst other things): (i) characteristic weak d–d transitions in the near-IR region which confirm the presence of osmium(III) centres; (ii) inter-valence charge-transfer bands in the near-IR region for the Os^{II}/Os^{III} states of the dinuclear complexes; and (iii) the presence of fully delocalised ligand-centred mixed-valence states such as sq/q and sq/sq/q for dinuclear and trinuclear complexes respectively.

Experimental

General details

Instrumentation used for routine spectroscopic and electrochemical studies has been described earlier,[29] as has the thermostatted optically transparent thin-layer electrode (OTTLE) cell used for the spectroelectrochemical studies.[29] The bridging ligands H_2L^1 (ref. 13) and H_6L^3 (ref. 30) were prepared according to the published methods; H_3L^2 and 2,2′-bipyridine (bipy) was purchased from Aldrich and used as received. $[Os(bipy)_2Cl_2]$ was prepared according to the published method.[31]

Preparations

$[Os(bipy)_2(cat)][PF_6]$. A mixture of $[Os(bipy)_2Cl_2]$ (0.095 g, 0.17 mmol) and catechol (0.020 g, 0.18 mmol) in aqueous ethanol (20 cm^3; 3 : 1 v/v) was heated to reflux under N_2 for 1 h, after which aqueous NaOH (0.020 g NaOH in 5 cm^3 water) was added dropwise. The resulting dark brown mixture was heated to reflux for 72 h. On cooling, aqueous NH_4PF_6 was added and air bubbled through the solution for 1 h. The resulting precipitate was collected by filtration and purified by column chromatography on alumina using MeCN–toluene (3 : 2, v/v) as eluent. The pure complex was isolated as a dark brown solid in 50% yield. ES-MS: *m*/*z* 609.3, $(M - PF_6)^+$. Found: C, 40.9; H, 2.5; N, 7.0. Required for $C_{26}H_{20}F_6N_4O_2OsP$: C, 41.3; H, 2.6; N, 7.4%.

$[\{Os(bipy)_2\}_2(L^1)][PF_6]_2$ $\{[Os_2(L^1)][PF_6]_2\}$. A mixture of $[Os(bipy)_2Cl_2]$ (0.61 g, 1.00 mmol) and H_4L^1 (0.10 g, 0.46 mmol) in aqueous ethanol (20 cm^3; 3 : 1 v/v) was heated to reflux under N_2 for 1 h, after which aqueous NaOH (0.020 g NaOH in 5 cm^3 water) was added dropwise. The resulting dark brown mixture was heated at reflux for 48 h. On cooling, aqueous NH_4PF_6 was added and air bubbled through the solution for 1 h. The resulting precipitate was collected by filtration and purified by column chromatography on alumina using MeCN–toluene (3 : 2, v/v) as eluent. The pure complex was isolated as a dark brown solid in 35% yield. ES-MS: *m*/*z* 1363.4, $(M - PF_6)^+$; 609, $(M - 2PF_6)^{2+}$. Found: C, 40.7; H, 2.1; N, 7.1. Required for $C_{26}H_{19}F_6N_4O_2OsP$: C, 41.4; H, 2.5; N, 7.4%.

$[\{Os(bipy)_2\}_2(L^2)][PF_6]_3$ $\{[Os_2(L^2)][PF_6]_3\}$. A mixture of $[Os(bipy)_2Cl_2]$ (0.50 g, 0.82 mmol) and H_3L^2 (0.12 g, 0.37 mmol) in EtOH–water (30 cm^3; 3 : 1 v/v) was heated to reflux for 45 minutes, after which aqueous NaOH (0.020 g NaOH in 5 cm^3 water) was added dropwise. The resulting purple mixture was heated to reflux for 15 h. After removal of the EtOH *in vacuo*, addition of aqueous NH_4PF_6 precipitated the complex as a dark blue powder which was collected by filtration and purified by column chromatography on alumina using CH_2Cl_2–MeOH (98 : 2, v/v) as eluent. Yield: 35%. ES-MS: *m*/*z* 1610.9, $(M - PF_6)^+$; 732.5, $(M - 2PF_6)^{2+}$; and 439.7, $(M - 3PF_6)^{3+}$. Found: C, 38.5; H, 2.5; N, 5.7. Required for $C_{59}H_{41}F_{18}N_8O_5P_3Os_2 \cdot 2H_2O$: C, 39.5; H, 2.5; N, 6.2%.

$[\{Os(bipy)_2\}_3(L^3)][PF_6]_3$ $\{[Os_3(L^3)][PF_6]_2\}$. This was prepared from $[Os(bipy)_2Cl_2]$ (0.20 g, 0.34 mmol) and H_6L^3 (0.040 g, 0.10 mmol) in exactly the same way as described above for $[\mathbf{Os_2}(L^1)][PF_6]_2$ except that the reaction time after addition of NaOH was 18 h. Purification by column chromatography on

alumina using MeCN–toluene (3 : 2, v/v) as eluent afforded the pure complex in 50% yield. ES-MS: m/z 984, $(M - 2PF_6)^{2+}$; 608, $(M - 3PF_6)^{3+}$. Found: C, 38.8; H, 2.6; N, 6.9. Required for $C_{78}H_{54}F_{18}N_{12}O_6P_3Os_3 \cdot 5H_2O$: C, 39.8; H, 2.7; N, 7.1%.

Crystal structure of $[Os(bipy)_2(cat)][PF_6]$

Crystal data. $C_{26}H_{20}F_6N_4O_2OsP$, $M = 755.6$, monoclinic, space group $C2/c$, $a = 11.8056(14)$, $b = 14.869(3)$, $c = 14.909(3)$ Å, $\beta = 104.011(10)°$, $V = 2539.3(7)$ Å^3, $T = 173$ K, $Z = 4$, μ(Mo-Kα) = 5.163 mm^{-1}. 8036 Reflections were measured with $2\theta_{max} = 55°$, which after merging afforded 2910 unique data ($R_{int} = 0.0253$). Final $wR2$ (all data) = 0.0549; $R1$ [selected data with $F > 4\sigma(F)$] = 0.0224. The molecule lies on a C_2 axis which bisects the catecholate ligand and passes through the Os atom. The instrument used was a Siemens SMART-CCD diffractometer. Software used: SHELXS 97 for structure solution;[32] SHELXL 97 for structure refinement;[32] SADABS for the absorption correction.[33]

CCDC reference number 186/2122.

See http://www.rsc.org/suppdata/dt/b0/b004858p/ for crystallographic files in .cif format.

Acknowledgements

We thank the EPSRC (UK) for Ph.D studentships (to A. M. B. and Z. R. R.), and Professor G. Lahiri (Indian Institute of Technology, Bombay) for valuable discussions.

References

1 C. G. Pierpont and C. W. Lange, *Prog. Inorg. Chem.*, 1994, **41**, 331.
2 A. B. P. Lever, H. Masui, R. A. Metcalfe, D. J. Stufkens, E. S. Dodsworth and P. R. Auburn, *Coord. Chem. Rev.*, 1993, **125**, 317.
3 S. I. Gorelsky, E. S. Dodsworth, A. B. P. Lever and A. A. Vlcek, *Coord. Chem. Rev.*, 1998, **174**, 469.
4 A. S. Attia and C. G. Pierpont, *Inorg. Chem.*, 1998, **37**, 3051.
5 O. S. Jung, D. H. Jo, Y. A. Lee, B. J. Conklin and C. G. Pierpont, *Inorg. Chem.*, 1997, **36**, 19.
6 M. Haga, E. S. Dodsworth and A. B. P. Lever, *Inorg. Chem.*, 1986, **25**, 447.
7 S. R. Boone and C. G. Pierpont, *Inorg. Chem.*, 1987, **26**, 1769.
8 S. Bhattacharya and C. G. Pierpont, *Inorg. Chem.*, 1992, **31**, 35.
9 S. Bhattacharya and C. G. Pierpont, *Inorg. Chem.*, 1991, **30**, 2906.
10 M. Haga, K. Isobe, S. R. Boone and C. G. Pierpont, *Inorg. Chem.*, 1990, **29**, 3795.
11 S. Bhattacharya, S. R. Boone, G. A. Fox and C. G. Pierpont, *J. Am. Chem. Soc.*, 1990, **112**, 1088.
12 M. Kurihara, S. Daniele, K. Tsuge, H. Sugimoto and K. Tanaka, *Bull. Chem. Soc. Jpn.*, 1998, **71**, 867.
13 L. F. Joulié, E. Schatz, M. D. Ward, F. Weber and L. J. Yellowlees, *J. Chem. Soc.*, *Dalton Trans.*, 1994, 799.
14 A. M. Barthram, R. L. Cleary, J. C. Jeffery, S. M. Couchman and M. D. Ward, *Inorg. Chim. Acta*, 1998, **267**, 1.
15 A. M. Barthram, R. L. Cleary, R. Kowallick and M. D. Ward, *Chem. Commun.*, 1998, 2695.
16 A. M. Barthram and M. D. Ward, *New J. Chem.*, 2000, **24**, 501.
17 M. D. Ward, *Inorg. Chem.*, 1996, **35**, 1712.
18 J. Fabian, H. Nakazumi and M. Matsuoka, *Chem. Rev.*, 1992, **92**, 1197.
19 R. J. Mortimer, *Chem. Soc. Rev.*, 1997, **26**, 147; R. J. Mortimer, *Electrochim. Acta*, 1999, **44**, 2971.
20 N. C. Harden, E. R. Humphrey, J. C. Jeffery, S.-M. Lee, M. Marcaccio, J. A. McCleverty. L. H. Rees and M. D. Ward, *J. Chem. Soc.*, *Dalton Trans.*, 1999, 2417.
21 C. G. Pierpont and R. M. Buchanan, *Coord. Chem. Rev.*, 1981, **38**, 44.
22 G. K. Lahiri, S. Bhattacharya, B. K. Ghosh and A. Chakravorty, *Inorg. Chem.*, 1987, **26**, 4324.
23 M. D. Ward, *Chem. Soc. Rev.*, 1995, **24**, 121.
24 A. Dei, D. Gatteschi and L. Pardi, *Inorg. Chim. Acta*, 1991, **189**, 125.
25 S. Decurtins, F. Felix, J. Ferguson, H. U. Güdel and A. Ludi, *J. Am. Chem. Soc.*, 1980, **102**, 4102.
26 M. M. Richter and K. J. Brewer, *Inorg. Chem.*, 1993, **32**, 2827.
27 E. M. Kober, K. A. Goldsby, D. N. S. Narayana and T. J. Meyer, *J. Am. Chem. Soc.*, 1983, **105**, 4303.
28 M. Haga, T. Matsumura-Inoue and S. Yamabe, *Inorg. Chem.*, 1987, **26**, 4148.
29 S.-M. Lee, R. Kowallick, M. Marcaccio, J. A. McCleverty and M. D. Ward, *J. Chem. Soc.*, *Dalton Trans.*, 1998, 3443.
30 H. Naarmann, M. Hanack and R. Mattmer, *Synthesis*, 1994, 477; D. R. Beattie, P. Hindmarsh, J. W. Goodby, S. D. Haslan and R. M. Richardson, *J. Mater. Chem.*, 1992, **2**, 1261.
31 M. J. Kendrick Geno and J. H. Dawson, *Inorg. Chim. Acta*, 1985, **97**, L41.
32 G. M. Sheldrick, SHELXS 97 and SHELXL 97, University of Göttingen, 1997.
33 G. M. Sheldrick, SADABS, A program for absorption correction with the Siemens SMART area-detector system, University of Göttingen, 1996.